Applied Physics Letters

Do we need perfect mixing between fuel and oxidizer to maximize the energy release rate of energetic nanocomposites?

Cite as: Appl. Phys. Lett. **122**, 011901 (2023); https://doi.org/10.1063/5.0133995
Submitted: 07 November 2022 • Accepted: 14 December 2022 • Published Online: 06 January 2023

Haiyang Wang, Yue Jiang, Yujie Wang, et al.

AIP Publishing

Applied Physics Letters ARTICLE scitation.org/journal/apl

Do we need perfect mixing between fuel and oxidizer to maximize the energy release rate of energetic nanocomposites?

Cite as: Appl. Phys. Lett. **122**, 011901 (2023); doi: 10.1063/5.0133995
Submitted: 7 November 2022 · Accepted: 14 December 2022 ·
Published Online: 6 January 2023

Haiyang Wang,[1] Yue Jiang,[2] Yujie Wang,[1] Dylan J. Kline,[1] Xiaolin Zheng,[2] and Michael R. Zachariah[1,a)]

AFFILIATIONS

[1]Department of Chemical and Environmental Engineering, University of California, Riverside, California 92521, USA
[2]Department of Mechanical Engineering, Stanford University, Stanford, California 94305, USA

[a)]Author to whom correspondence should be addressed: mrz@engr.ucr.edu

ABSTRACT

It is well accepted that close assembly between a fuel and an oxidizer can increase the interfacial contact-area and reduce the diffusion distances, which can significantly promote a heterogeneous reaction. However, we recently observed for nanocomposites of Al/PVDF (aluminum/polyvinylidene fluoride), that if we separated some of the PVDF to form a laminated structure, the flame propagation rate is significantly increased compared to the homogenous case. To probe the mechanism behind this, we used functionalized aluminum nanoparticles to create microsized aggregates of Al-rich and PVDF-rich regions to induce the inhomogeneity and also fabricated Al/PVDF laminate structure films to control the inhomogeneity systematically. The result demonstrates that the inhomogeneous mixing between Al and PVDF can significantly increase the flame front corrugation (burning area). This presumably occurs due to variations in the microburn rate (local burn velocity vectors at the flame front on the microscale). The benefit of the enhanced flame area can apparently overcome the effects of the decrease in the contact area, leading to enhanced burning for an inhomogeneously mixed system. Finally, fluorocarbon functionalization of Al particles can further increase the microburn rate.

Close assembly between a fuel and an oxidizer can significantly enhance heterogeneous reactions by increasing the interfacial contact area and reducing the diffusion distance between reactants. For example, using aluminum nanoparticles (Al NPs) to replace conventional microsized Al as a fuel in reactive metal composites can increase the burn rate by 1000×.[1–4] However, we have also recently observed that, for Al/polyvinylidene fluoride (PVDF), if the fuel (Al) and oxidizer (PVDF) are separated in a laminated structure, the burn rate was higher than the homogeneously mixed samples.[5] The resolution of the imaging apparatus at the time limited our view of the flame front and, therefore, we could only make broad conclusions about the mechanisms driving the enhanced reactivity. In this work, we modified the fabrication procedure of the reactive Al/PVDF laminates to create structures that could be more easily resolved with our imaging apparatus. We then modified the structure of the composite to assess the impact of fuel/oxidizer mixing on composite reactivity.

To better resolve the role of inhomogeneity on reactivity, the Al NPs were functionalized to create microsized aggregates of Al-rich and PVDF-rich regions which could be resolved by our imaging apparatus. Four different functional groups were used to functionalize the Al NPs' (70 nm, US Nano Research, 72.5 wt. % active Al content) surface via a silylation reaction: two hydrocarbon-terminated chains [triethoxy(octyl)silane ($C_8H_{17}Si(OC_2H_5)_3$, OTS) and hexadecyltrimethoxysilane ($C_{16}H_{33}Si(OCH_3)_3$, HDTS] and two hydro-fluorocarbon chains [1H,1H,2H,2H-perfluorooctyltriethoxysilane ($C_8H_4F_{13}Si(OC_2H_5)_3$, FOTS) and 1H,1H,2H,2H-perfluorodecyltriethoxysilane ($C_{10}H_4F_{17}Si(OC_2H_5)_3$, FDTS)] [Figs. 1(a) and S1]. The detailed recipe of surface functionalization can be found in previous works.[6,7] The coating materials are ∼7.5 wt. % based on our previous estimation.[6] These functionalized Al NPs (Al@OTS, Al@HDTS, Al@FOTS, and Al@FDTS) and the reference Al NPs were mixed in a PVDF-containing solution (solvent: DMF, concentration: 50 mg/mL) to form inks for printing different Al/PVDF films (Hyrel Printer),[8] and the cross-sectional SEM images are shown in Figs. 1(b)–1(f), respectively. All the functionalized films were fabricated to have the same thickness of 41 μm, which is slightly thicker than the reference Al/PVDF film (37 μm).

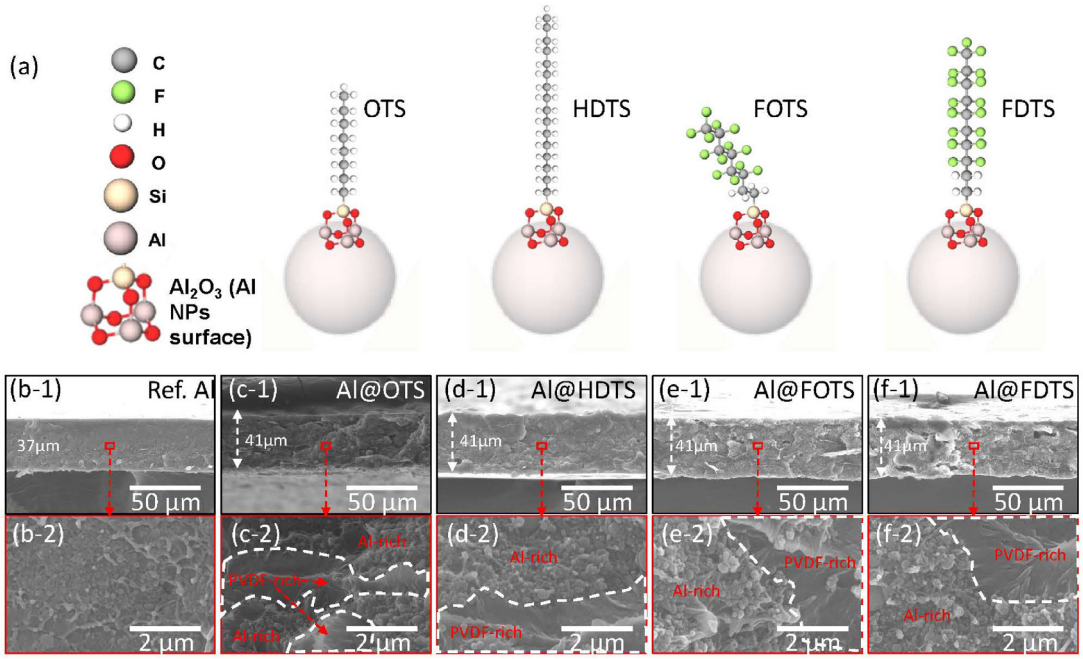

FIG. 1. Schematic showing different functionalized Al NPs (a). Low (b-1)–(f-1) and higher (b-2)–(f-2) cross-sectional SEM images of different Al/PVDF films with reference Al (b), Al@OTS (c), Al@HDTS (d), Al@FOTS (e), and Al@FDTS (f). Note: white-dashed regions are the PVDF-rich domains.

A more important difference between the reference and functionalized Al/PVDF films is the mixing homogeneity between Al and PVDF. Reference Al/PVDF films (which did not have particle surface modifications) had Al NPs homogeneously dispersed in the film [Figs. 1(b-1) and 1(b-2)]. However, the Al/PVDF films prepared using functionalized Al NPs had inhomogeneities that were produced by precipitating microsized PVDF domains in the film [Figs. 1(b-1)–1(f-1) and 1(b-2)–1(f-2)]. The functionalized Al NPs have a non-polar surface as shown in Fig. 1(a) that cannot be dispersed well in the polar solvent of DMF. This mismatch in surface polarity creates an emulsion containing PVDF domains and Al NP aggregates which remain present after the solvent is evaporated (as a part of the printing process). The resulting film has discrete locations where the composite mixture is either fuel-rich (Al NP aggregates) or fuel-lean (PVDF domains) [Figs. 1(b-2)–1(f-2)]. All the functionalized Al/PVDF films have enhanced ductility but lower Young's modulus (Fig. S2) compared to the reference films due to the embedded pure PVDF phases.

To probe the effects of the mixing between Al and PVDF on the flame propagation in detail, the films were mounted on a three-axis translational stage between two camera systems with different magnifications. On the far side, a macroscopic imaging high-speed camera (Miro M110) captures the global burning event of a whole film (~1.5 cm long) at a window size of 640 × 200 pixels and a resolution of ~80 μm/pixel [Fig. 2(a)]. On the near side, a microscopic imaging system images the middle of the film at a window size of 448 × 800 pixels and a resolution of ~2.2 μm/pixel. The films were ignited by a nichrome wire and burned in an inert environment (1 atm Ar).

From the macroscopic and microscopic videos, the global burn rate [Fig. 2(b)] and microburn rate [Fig. 2(b)] can be obtained, respectively. The global burn rate is defined as (film length)/(burn time). The microburn rate is determined under microscopic imaging and is measured using custom software that has been previously reported by Kline *et al.*[9] In particular, for two consecutive frames [Fig. 2(b), frames 1 and 2], we take each of the points in the flame

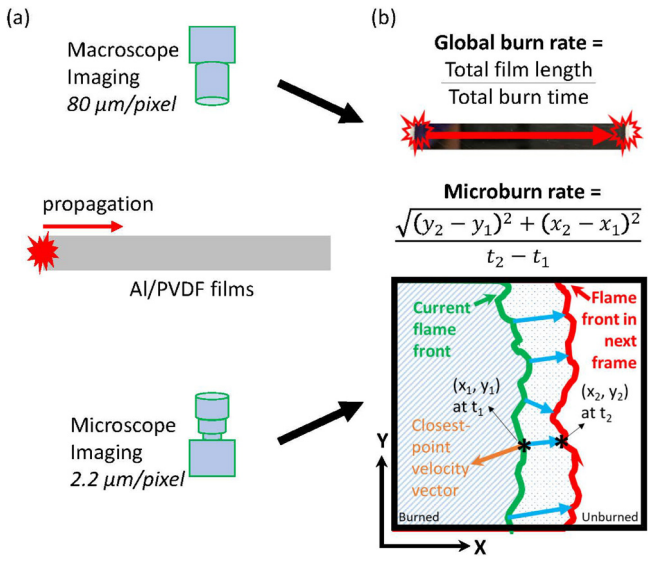

FIG. 2. Schematic showing (a) macroscopic and microscopic imaging of Al/PVDF film and the measurement approaches (b) of global burn rate and microburn rate.

front in frame 1 [current front in Fig. 2(b)] and match it to the closest point in the flame front in frame 2 [next frame in Fig. 2(b)] to calculate the distance between the two points. We divide this distance by the time per frame (1/fps) to obtain the local velocity. The flame temperature is obtained via a color pyrometry method that can be found in detail in our previous studies.[10,11] Briefly, three channel intensity (RGB: red, green, and blue) ratios are extracted to represent the reaction flame temperature after calibration with a blackbody source (Mikron M390). The flame temperatures are averaged based on all available points throughout three whole burning events and the mean value with standard deviation is utilized for experimental calculations.

The global burn rates and flame temperature are obtained from the macroscopic burning videos and the results are shown in Fig. 3(a). The global burn rate of fluorocarbon functionalized Al/PVDF films (Al@FOTS and Al@FDTS) is ∼10–12 cm/s, which is ∼2× higher than the reference Al/PVDF and hydrocarbon functionalized Al/PVDF (∼6 cm/s). The flame temperature of all the films is ∼1600 K, and there is only a marginal difference in the measured densities (measured gravimetrical) of the films (∼1.5–1.9 g/cm^3). The heat flux to the unburned region can, therefore, be estimated as shown in Fig. 3(b) as proportional to density × burn rate × temperature rise [details can be found in Eqs. (S1)–(S3) in the supplementary material].[12] The heat flux of fluorocarbon functionalized Al/PVDF is found to be ∼150% higher than other films. The different Al/PVDF films are also ignited and burned in a constant-volume vessel, the peak pressure, pressure rise rate, and ignition delay time were obtained using the method

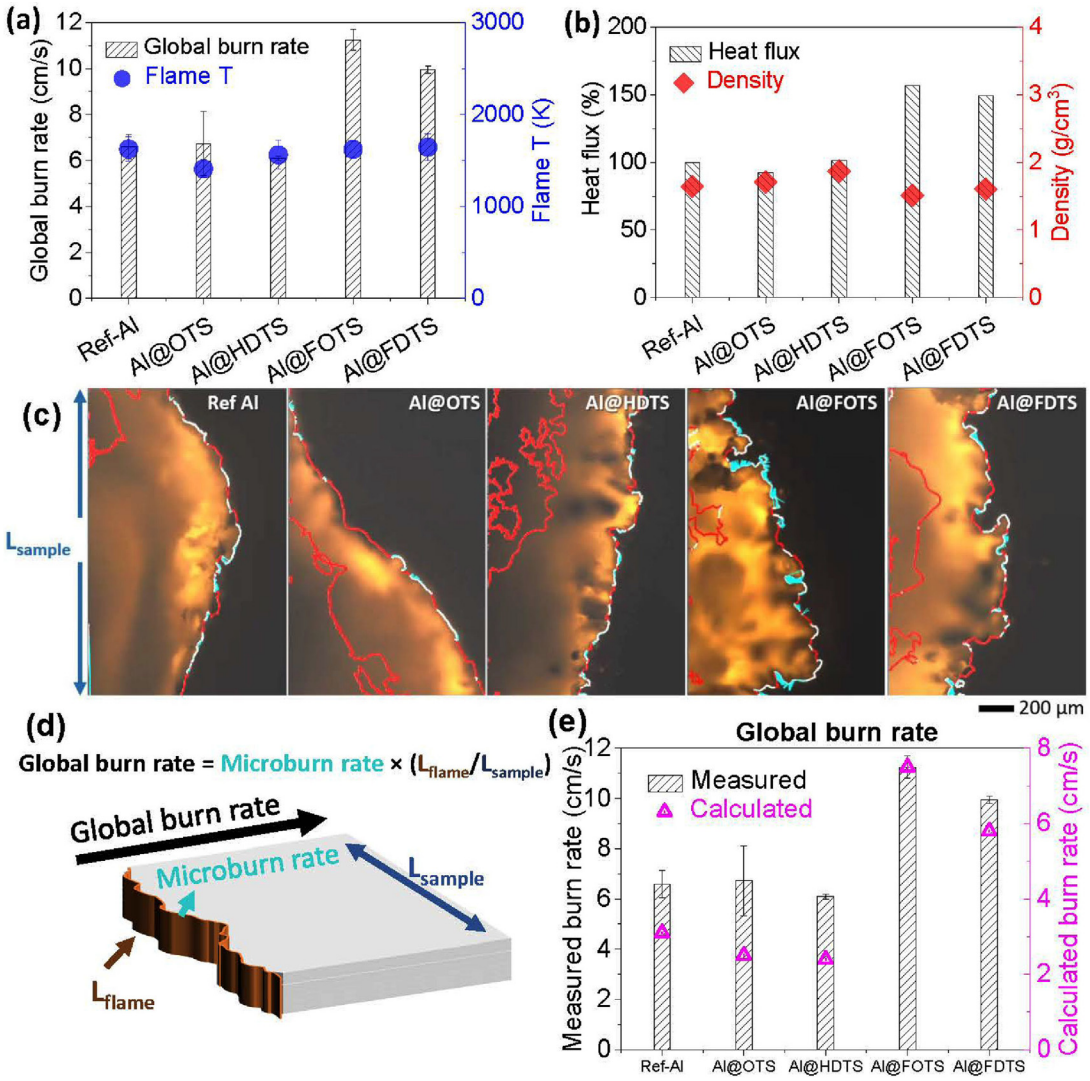

FIG. 3. Measured global burn rate and flame temperature (a) as well as the density and heat flux (b) of different Al/PVDF films. The microscopic snapshots (c) show the corrugation of the flame and indicate the typical microburn velocity vectors of different Al/PVDF films, more details can be found in Video S1. The relationship between global burn rate and microburn rate (d). The comparison of measured and calculated global burn rate (e). Multimedia view: https://doi.org/10.1063/5.0133995.1

reported before and shown in Fig. S3.[13,14] Consistently, the Al@FOTS/PVDF is the most reactive among all the films, which is ~2× more reactive (pressure rise rate) compared to the reference Al/PVDF.

As the cross-sectional SEM images in Fig. 1 show, both hydrocarbon and fluorocarbon functionalized Al yielded inhomogeneous Al/PVDF films, while only the latter had a higher global burn rate and heat flux. Typical snapshots of the microscopic videos are shown in Fig. 3(c) (Multimedia view). The microburn rates of Al@FOTS/PVDF and Al@FDTS/PVDF are about two times of the reference Al/PVDF film, while the hydrocarbon functionalized Al/PVDF films have slightly higher microburn rate compared to reference Al/PVDF film (more details can be found in Table S1). Moreover, we also notice the different flame fronts of these Al/PVDF films from the microscopic imaging videos. As shown in Fig. 3(d), the width of the film is defined as L_{sample}, and the length of the flame front is defined as L_{flame}. Figure 3(c) clearly shows that the length of the flame front of two fluorocarbon functionalized Al/PVDF films is significantly higher (>150%) than the reference Al/PVDF, confirming the larger burning surface area, while the hydrocarbon functionalized Al/PVDF films has similar flame front corrugation (L_{flame}/L_{sample}) compared to the reference Al/PVDF. As shown in Fig. 3(d), the global burn rate can be estimated by multiplying the microburn rate and the ratio of L_{flame}/L_{sample}.[15] Even though the calculated global burn rates are lower than the measured burn rates [Fig. 3(e)], the trend matches well between each other, further confirming that both microburn rate and flame front corrugation (L_{flame}/L_{sample}) contribute to the global burn rate increase in these fluorocarbon functionalized Al/PVDF films.

To further confirm the relationship between inhomogeneity and flame corrugation, we also printed Al/PVDF composite layers with PVDF layers among them, with the same total amount of Al NPs and PVDF compared to the uniform Al/PVDF film. The cross-sectional SEM images of the printed uniform and laminate Al/PVDF films are shown in Figs. 4(a) and 4(b), respectively. As the EDS mapping results [Fig. 4(c)] demonstrate, there are three Al-rich layers and three PVDF layers in alternating layers (six layers total). Figures 4(d)–4(g) (Multimedia view) demonstrate the macroscopic and microscopic combustion behaviors of the uniform and laminate Al/PVDF films. Even though they have the same composition and roughly the same density, the global burn rate of laminate Al/PVDF is ~12 cm/s [Fig. 4(e)], which is almost 2× higher than the uniform Al/PVDF [Fig. 4(d)]. The flame of the laminate Al/PVDF is also much brighter and wider. When the flame front is zoomed-in, we observe a smooth flame front for the uniform Al/PVDF film [Fig. 4(f)] but a much more corrugated flame front with a significantly higher microburn rate for the laminate Al/PVDF film [Fig. 4(g)].

Thus, one conclusion is that the inhomogeneous mixing between Al and PVDF induced by the fluorocarbon functionalized Al NPs significantly increases the flame front corrugation, which in turn, promotes a high global burn rate. A new question now arises from this conclusion: why is the burn rate of the fluorocarbon functionalized Al/PVDF films faster than the hydrocarbon functionalized Al/PVDF films (Fig. 3) if they have similar inhomogeneity (Fig. 1)? To further probe this, we also prepare laminated Al/PVDF films that have six layers with Al@OTS [Fig. S4(b)] and Al@FOTS [Fig. S4(c)]. The flame front corrugation and microburn rate data of these two laminates are summarized in Fig. 4(h) with the above-mentioned reference laminate and other single layer Al/PVDF films. The Al@OTS/PVDF and

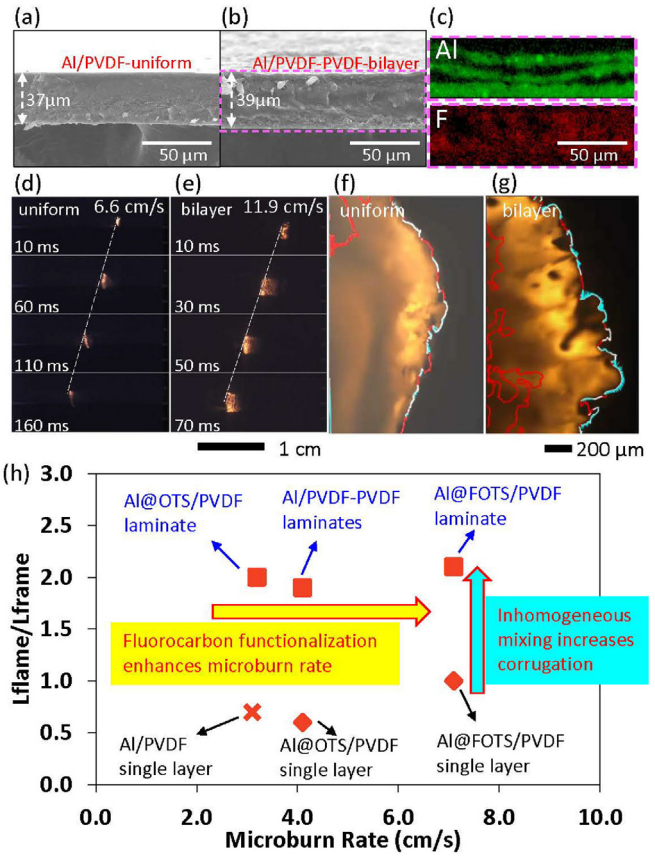

FIG. 4. SEM image comparison between uniform (a) and laminated (b), three bilayers Al/PVDF films. The EDS results (c) of laminated Al/PVDF show the Al-rich and PVDF-rich layers. Macroscopic (d) and (e) and microscopic (f) and (g) burning snapshots comparison between uniform (d) and (f) and laminated (e) and (g) Al/PVDF films, more details can be found in Video S2. Summary about corrugation (L_{flame}/L_{sample}) and microburn rate of different Al/PVDF films (h). Multimedia view: https://doi.org/10.1063/5.0133995.2

Al@FOTS/PVDF laminate films shows a L_{flame}/L_{sample} value of ~2, which is ~2× higher than the value of 0.7 of pure Al/PVDF, further confirming the inhomogeneous mixing can efficiently increase the flame front corrugation. However, similar to the single layer of Al@OTS/PVDF, the microburn rate of Al@OTS/PVDF laminate films is only ~3 cm/s, which is lower than half of Al@FOTS/PVDF laminate films. From previous studies,[6,7] the fluorocarbon functionalized Al NPs have significantly higher reactivity compared to bare Al, as a result, the microburn rate is also higher.

These results confirm that fluorocarbon functionalization on Al NPs not only induces inhomogeneity in Al/PVDF films, creating a more corrugated flame front, but also increases the microburn rate, resulting in the highest burn rate in the series of Al/PVDF films.

We believe that these results demonstrate that inhomogeneous mixing can significantly increase the flame front corrugation stemming from the small variations in the microburn rate. The positive impact of the increased burn area on the overall burn rate can also seemingly overcome the negative impact of reduced reactant mixing;

the combination of both effects yields an enhanced burn rate for the inhomogeneous system.

See the supplementary material for schematic showing different functionalized aluminum nanoparticles. Stress–strain curves and constant-volume vessel test results of different Al/PVDF films. Summary of the measured global burn rate, microburn rate, corrugations, flame temperature, density, and heat flux of all the Al/PVDF films used in this study.

The authors gratefully acknowledge the support from AFOSR and ARO. They also thank the CFAMM at the University of California, Riverside, for their microscopy support. Stanford authors were supported by the Office of Naval Research managed by Chad Stoltz under Agreement No. N00014-19-1-2085.

AUTHOR DECLARATIONS

Conflict of Interest

The authors have no conflicts to disclose.

Author Contributions

Haiyang Wang, Yue Jiang, and Yujie Wang contributed equally to this work.

Haiyang Wang: Conceptualization (lead); Data curation (lead); Investigation (lead); Methodology (equal); Project administration (lead); Supervision (lead); Writing – original draft (lead); Writing – review & editing (equal). **Yue Jiang:** Data curation (equal); Writing – original draft (lead); Writing – review & editing (equal). **Yujie Wang:** Data curation (equal); Writing – review & editing (equal). **Dylan Jacob Kline:** Data curation (equal); Writing – review & editing (equal). **Xiaolin Zheng:** Conceptualization (equal); Funding acquisition (equal); Writing – review & editing (equal). **Michael Zachariah:** Conceptualization (lead); Data curation (equal); Investigation (lead); Methodology (equal); Project administration (lead); Supervision (lead); Writing – original draft (equal); Writing – review & editing (equal).

DATA AVAILABILITY

The data that support the findings of this study are available from the corresponding author upon reasonable request.

REFERENCES

[1]R. A. Yetter, G. A. Risha, and S. F. Son, "Metal particle combustion and nanotechnology," Proc. Combust. Inst. **32**(2), 1819–1838 (2009).
[2]C. E. Aumann, G. L. Skofronick, and J. A. Martin, "Oxidation behavior of aluminum nanopowders," J. Vac. Sci. Technol. B **13**(3), 1178–1183 (1995).
[3]G. Young, K. Sullivan, M. R. Zachariah, and K. Yu, "Combustion characteristics of boron nanoparticles," Combust. Flame **156**(2), 322–333 (2009).
[4]E. L. Dreizin, "Metal-based reactive nanomaterials," Prog. Energy Combust. Sci. **35**(2), 141–167 (2009).
[5]X. Li, P. Guerieri, W. Zhou, C. Huang, and M. R. Zachariah, "Direct deposit laminate nanocomposites with enhanced propellent properties," ACS Appl. Mater. Interfaces **7**(17), 9103–9109 (2015).
[6]Y. Jiang, Y. Wang, J. Baek *et al.*, "Ignition and combustion of perfluoroalkyl-functionalized aluminum nanoparticles and nanothermite," Combust. Flame **242**, 112170 (2022).
[7]J. Baek, Y. Jiang, A. R. Demko *et al.*, "Effect of fluoroalkylsilane surface functionalization on boron combustion," ACS Appl. Mater. Interfaces **14**, 20190 (2022).
[8]J. Shen, H. Wang, D. J. Kline *et al.*, "Combustion of 3D printed 90 wt. % loading reinforced nanothermite," Combust. Flame **215**, 86–92 (2020).
[9]D. J. Kline, M. C. Rehwoldt, H. Wang, N. E. Eckman, and M. R. Zachariah, "Why does adding a poor thermal conductor increase propagation rate in solid propellants?," Appl. Phys. Lett. **115**(11), 114101 (2019).
[10]R. J. Jacob, D. J. Kline, and M. R. Zachariah, "High speed 2-dimensional temperature measurements of nanothermite composites: Probing thermal vs. gas generation effects," J. Appl. Phys. **123**(11), 115902 (2018).
[11]D. J. Kline, M. C. Rehwoldt, J. B. DeLisio *et al.*, "In-operando thermophysical properties and kinetics measurements of Al-Zr-C composites," Combust. Flame **228**, 250–258 (2021).
[12]H. Wang, D. J. Kline, M. C. Rehwoldt, and M. R. Zachariah, "Carbon fibers enhance the propagation of high loading nanothermites: *In situ* observation of microscopic combustion," ACS Appl. Mater. Interfaces **13**, 30504 (2021).
[13]S. Deng, Y. Jiang, S. Huang, X. Shi, J. Zhao, and X. Zheng, "Tuning the morphological, ignition and combustion properties of micron-Al/CuO thermites through different synthesis approaches," Combust. Flame **195**, 303–310 (2018).
[14]S. Huang, S. Deng, Y. Jiang, and X. Zheng, "Experimental effective metal oxides to enhance boron combustion," Combust. Flame **205**, 278–285 (2019).
[15]H. Wang, P. Biswas, and M. R. Zachariah, "Direct imaging and simulation of the interface reaction of metal/metal oxide nanoparticle laminates," J. Phys. Chem. C **126**, 8684 (2022).